Dynamics and Ligand-Induced Solvent Accessibility Changes in Human Retinoid X Receptor Homodimer Determined by Hydrogen Deuterium Exchange and Mass Spectrometry†

Xuguang Yan,‡ David Broderick,§ Mark E. Leid,|| Michael I. Schimerlik,*,§ and Max L. Deinzer*,‡

Departments of Chemistry, Biochemistry and Biophysics, and Pharmaceutical Science, Oregon State University, Corvallis, Oregon 97331

Received July 31, 2003

ABSTRACT: Receptors for retinoic acid act as ligand activated transcription factors. The three-dimensional structure of the retinoid X receptor (RXR) ligand binding domain has been determined, but little information is available concerning the properties of the protein in solution. Hydrogen/deuterium exchange followed by electrospray ionization mass spectrometry was used to probe the solution conformation of the recombinant human RXRα homodimer ligand binding domain in the presence and absence of 9-*cis*-retinoic acid (9-*cis*-RA). Within the experimental time domain (0.25−180 min), about 20 amide hydrogens showed decreased exchange rates in the presence of saturating concentrations of 9-*cis*-RA as compared to those found for the homodimer in the absence of ligand. Most of the amides were located in peptides derived from regions of the protein shown by the X-ray structure to interact with the bound ligand: the amino termini of helices 3 and 9, the two β sheets, helix 8, the H8−H9 loop, and the carboxyl terminus of helix 11. Unexpectedly, protection was also observed in peptides derived from helices 7, 10, 11, and the H7−H8 and H10−H11 loops, regions that are not directly in contact with bound 9-*cis*-RA. These results suggest that the binding of ligand results in additional effects on the conformation or dynamics of the homodimer in solution as compared to those observed for the X-ray structure. Overall, the change in deuterium exchange induced by the binding of 9-*cis*-RA correlated reasonably well with changes in hydrogen bonding, residue depth, and/or solvent accessibility predicted from the crystal structure.

Receptors for retinoids belong to the class of proteins that act as ligand regulated transcription factors. They are composed of retinoid X receptors (RXR)[1] and retinoic acid receptors (RAR) with each class having α, β, and γ isotypes (*1*). The ligand specificities and signaling properties vary with respect to each respective protein isotype. The receptors are organized structurally into a ligand independent amino terminal transcriptional domain (A/B) followed by a DNA binding domain (C), hinge region (D), and a ligand binding domain (E) that overlaps the dimerization interface and ligand dependent transcriptional activation function.

The purified E domain from the RXR has been shown to exist as either dimers or tetramers in solution (*2*), and the crystal structures of both have been determined (*3*, *4*). Addition of the agonist 9-*cis*-RA induces the dissociation of the tetrameric state to form dimers (*2*). The crystallography data (*5*) have also shown that the binding of agonists to the dimeric RXR leads to large conformational changes in the protein including the movement of helix 12 to cover the occupied ligand binding site and create a new surface that can then interact with coactivators, presumably resulting in the activation of transcription (*6*, *7*).

The crystallographic studies have resulted in a wealth of information leading to the development of a mechanistic model for receptor signal transduction via RXR homodimers (*5*) or heterodimers with other transcription factors (*8*) and a possible role of the RXR tetramer in the cell as an inactive storage form for RXRs (*3*). At this time, little is known concerning the solution dynamics of the free protein or the complex of the RXR homodimer with ligands.

The hydrogen/deuterium (H/D) exchange information on peptide amide hydrogens can reflect protein dynamic features (*9*, *10*), and the H/D method has been used to probe protein−ligand interactions (*11*−*13*). Presumably, solvent accesses flexible or dynamic regions of a protein more readily, and such events are reflected by fast deuterium exchange. Regions of limited flexibility may be less penetrable by solvent, but slow deuterium exchange may also be a reflection of greater stability of the hydrogen bonds. Thus, structural changes that occur in the protein from ligand

† This work was supported by the NIH/NIEHS Grants ES00040 to M.I.S. and M.L.D. and NIDDK Grant RO1 DK60613 to M.I.S.

* Corresponding authors. (M.L.D.) E-mail: max.deinzer@orst.edu. Fax: (541) 737-0497. Phone: (541) 737-1773. (M.I.S.) E-mail: schimerm@onid.orst.edu. Fax: (541) 737-0481. Phone: (541) 737-2029.

‡ Department of Chemistry.

§ Department of Biochemistry and Biophysics.

|| Department of Pharmaceutical Science.

[1] Abbreviations: CHAPS, 3-[(3-cholamidopropyl)dimethyl-ammonio]-1-propanesulfonate; CID, collisionally induced dissociation; 9-*cis*-RA, 9-*cis* retinoic acid; EDTA, ethylenediamine tetraacetic acid; ESI-MS, electrospray ionization mass spectrometry; H/D, hydrogen/deuterium; HPLC, high performance liquid chromatography; LBD, ligand binding domain; RMSD, root-mean-square deviation; RXR, retinoid X receptor; TCEP, tris(2-carboxyethyl)phosphine hydrochloride; TFA, trifluoroacetic acid.

10.1021/bi030183c CCC: $27.50
Published on Web 01/03/2004

binding should be evident from an analysis of the H/D exchange behavior. Detecting amide deuterium exchange information by mass spectrometry is a powerful new technique (*14*, *15*). It provides an experimental approach for examining solvent accessibility of protein backbone amide hydrogens and may therefore give information on the environment of distinct regions of the protein and how that environment is affected by the binding of ligands. In this paper, the H/D exchange properties of the dimeric RXRα E domain are reported, and the effects of the agonist 9-*cis*-RA on the kinetics of exchange are described. In addition to the protection of residues that form direct contacts with the ligand as shown in the crystal structure, the kinetic properties of other protein regions not predicted from the crystal structure were also found to be modified. These results, and comparison with the crystal structure, may result in an increase in understanding of the properties of the RXR homodimer in solution and contribute to a more complete understanding of retinoid signal transduction mechanisms.

EXPERIMENTAL PROCEDURES

The protein was expressed and purified as described by Egea (*2*). Briefly, the pET15b plasmid coding for N-terminal 6xHis-tagged fusion protein that encodes T223 to T462 of the human RXRα ligand binding domain (LBD) was overexpressed in *Escherichia coli*, which was grown at 37 °C to an absorbance (A_{600}) 0.6−0.8 followed by induction of protein synthesis at 25 °C by 0.8 mM IPTG for 5 h. After centrifugation and washing, cell pellets were lysed by sonication, and the His-tagged protein was purified by chromatography (150 mM imidazole, 0.3 M KCl, 50 mM potassium phosphate, pH 7.0) on cobalt-containing affinity resins (Talon, Clonetech). The protein was eluted into a solution containing 20 μL of 500 mM EDTA and 10 μL of 100mM CHAPS to a final volume of 2 mL of solution at which point a concentration of 5 mM EDTA and 0.5 mM CHAPS was reached. The His-tag was removed by thrombin digestion at 4 °C (48 h, 1 unit/mg protein) followed by purification on an analytical Superdex S200-HR 10/30 size exclusion column (0.5 M KCl, 0.5 mM CHAPS, 1 mM TCEP, 50 mM potassium phosphate, pH 7.4) to obtain a purified human RXRα homodimer that was used for all experiments. Protein concentration was determined by the Bradford assay (*16*), and the purity was judged by sodium dodecyl sulfate−polyacrylamide gel electrophoresis as well as by mass spectrometry. The purity was estimated as over 95%. Nondenaturing ESI-MS analysis of RXRα was carried out on a Q-Tof (Micromass) mass spectrometer by direct infusion in nanospray, where prior protein buffer exchange was applied against 50 mM ammonium acetate (pH 6.8) with a Biomax membrane ultrafilter (5 K MW cutoff, Millipore Co.).

The purified RXRα homodimer (45 μM) was incubated at 25 °C in an aqueous solution consisting of 0.5 M KCl, 0.5 mM CHAPS, 1mM TCEP, and 50 mM potassium phosphate buffer (pH 7.4) for 30 min with and without 9-*cis*-RA (Sigma). Hydrogen exchange was initiated by 10-fold dilution of the protein in the same buffer but in D_2O (pD 7.0) at 25 °C with and without ligand. Protein−ligand equilibration was achieved by adding 2 μL of ligand (4 mM 9-*cis*-RA in ethanol) into 35 μL of protein buffer so that the final concentration of ligand was over 5 times that of the dimeric protein. The ligand (3 μL) was also added into the D_2O buffer (100 μL) for deuterium exchange in the presence of ligand. Deuterium exchange in the absence of ligand was determined after addition of the same amount of ethanol to the protonated or deuterated protein buffer solution. This small amount of ethanol did not affect the protein secondary structure as indicated by far UV−CD spectroscopy.

Hydrogen exchange was allowed to proceed for various periods of time. At specified times, 50 μL aliquots were taken and added to a prechilled tube containing 50 μL of 0.17% phosphoric acid to quench the reaction (pH 2.6). The quenched sample was either immediately subjected to LC-ESI-MS (LCQ) analysis under ice bath conditions or digested with immobilized pepsin (protein/enzyme 1:2 molar ratio) for 2 min and then frozen in liquid nitrogen for later analysis.

Peptic peptides were analyzed by LC-ESI-MS (LCQ) as rapidly as possible under optimum quench conditions (0 °C, pH 2.6). The deuterium level for each peptide was determined from the difference in centroided masses between the deuterated and the nondeuterated fragments. The fully deuterated protein sample was used as a control to estimate deuterium loss during protein digestion and the LC-MS step for the nonliganded protein and liganded protein. Back-exchange of hydrogen isotope in each peptic fragment was determined from the theoretical mass for the fully deuterated fragments and the experimentally measured molecular mass. The fully deuterated protein was obtained by denaturing it in D_2O containing 8 M urea-d_4 and allowing exchange for 5 h at room temperature and then renaturing it in D_2O buffer by removing urea-d_4 with a Biomax membrane ultrafilter. It should not be necessary to adjust for back-exchange when comparing molecular weights for the corresponding deuterated peptides in the nonliganded protein and the liganded protein complex, as the back-exchange should be the same under identical conditions. However, minimizing back-exchange is important to avoid losing important deuterium exchange information. The average back-exchange for the 61 peptic peptides that were analyzed was 15.3% with a range of 5.3−25.1%. The error of mass measurement on the LCQ mass spectrometer is ± 0.25 Da; thus, differences of <0.3 Da between the corresponding peptides of the deuterated protein and the protein−9-*cis*-RA complex was not considered significant. Protein molecular weight was determined by deconvoluting ESI multiple charge states using Bioworks 2.0 software (for LCQ data) and Masslynx 4.0 (for Q-Tof data). The entire set of experiments was repeated and found to give similar values.

The secondary structure of the protein was determined by the DSSP program (*17*), and virtual hydrogen bonding sites were identified with the HBPlus 3.15 program (*18*). The solvent accessible surface area was calculated by the web-based program Getarea 1.1 (http://www.scsb.utmb.edu/cgi-bin/get_a_form.tcl) (*19*); the corresponding percentage was calculated relative to the maximum surface areas of the residues (*20*). The three-dimensional structure comparison was carried out by the Local-Global Alignment program (http://predictioncenter.llnl.gov/local/lga/) (*21*). The depth of each residue was defined as described by Chakravarty and Varadarajan (*22*). Briefly, the depth of an atom in the protein crystal is its average distance from the nearest surface water molecule computed from a rotation of the protein through a random angle about its axis. A number of iterations (i.e.,

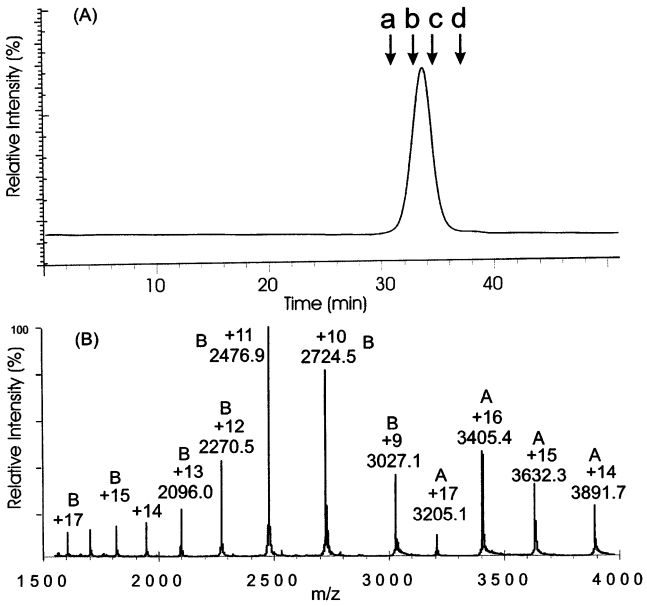

FIGURE 1: Size exclusion chromatograph of recombinant human RXRα LBD dimer (33.6 min), tetramer (a, 30.7 min) and molecular weight standards (b, albumin, MW 67 000, 32.7 min; c, ovalbumin, MW 43 000, 34.6 min; and d, chymotrypsinogen A, MW 25 000, 36.9 min) on analytical Superdex S200-HR 10/30 (Pharmacia) equilibrated with 0.05 M potassium phosphate, 0.5 M KCl, 1 mM TCEP, 0.5 mM CHAPS, pH 7.4 monitored by absorbance at 280 nm (A). ESI-MS spectrum of RXRα homodimer under nondenaturing conditions (50 mM ammonium acetate, pH 6.8) by direct infusion nanospray showing two charge state envelops, dimer group (A14−A17 [numbers refer to charges]) and monomer group (B9−B17 [numbers refer to charges]) (B).

rotation and translation, which generate a configuration of water molecules around the protein along with the removal of water molecules from cavities) are performed to convergence, so that the coefficient of variance of depth for each atom is less than a predetermined value. The analysis of the previous parameters is based on the crystallographic data for the ligandbound structure (PDB: 1FBY) as well as the nonliganded structure (PDB: 1LBD). The homodimer coordinates for the nonliganded structure were provided by Bourguet et al. (*4*).

RESULTS

The size of the introduced His-tag is small, but it was believed that it would cause structural changes (*23*), and it was therefore removed prior to conformational studies by hydrogen/deuterium exchange. Size exclusion chromatographic analysis showed a single peak whose retention time, when compared to a series of standard macromolecules, indicated that the molecular weight of the expressed protein was about 54 kDa (Figure 1A), thereby confirming that the purified protein was indeed a homodimer. This noncovalent homodimer dissociated during LC-ESI MS and showed the molecular weight only for the monomer. The protein−ligand complex with 9-*cis*-RA also dissociated during this step, although the ligand normally binds tightly in solution (K_d = 43 ± 3 nM) as shown by fluorescence titration. However, the noncovalent homodimer was observed by direct infusion ESI-MS analysis under nondenaturing conditions (Figure 1B), although the charge state envelope of dissociated monomer also appeared. The ligand−protein complex could not be observed under these conditions.

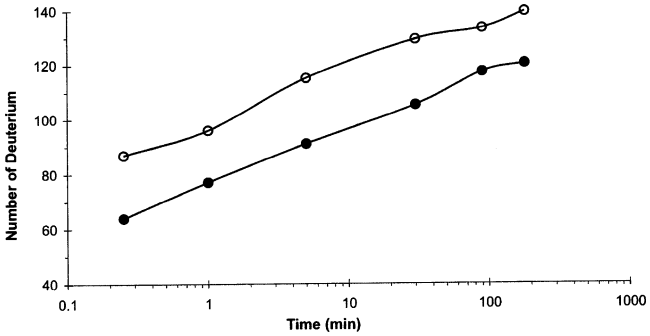

FIGURE 2: Deuterium levels at amide bonds in the human RXRα LBD homodimer (open circles) and the homodimer complex with 9-*cis*-RA (solid circles) as a function of deuterium exchange in time (0.25−180 min). Data represent the average of two experiments with a typical deviation of about 5% between measurements. No correction was made for proton back-exchange.

The amino acid sequence of the purified protein was verified through mass analysis of tryptic and peptic peptides by ESI-MS. Before removal of the His-tag, the molecular weight was found to be 28,705 ± 0.8 Da, which was 131 Da less than that calculated from the encoded protein sequence; the difference is due to the loss of the N-terminal methionine. After removal of the His-tag, the molecular weight was found to be 27,235 ± 1.0 Da, which matched the encoded sequence plus the addition of three amino acids (GSH) as a result of thrombin cleavage near the N-terminus of the protein. The protein was completely mapped out by mass spectrometry and collision-induced dissociation (CID) MS/MS of the proteolytic fragments.

Each subunit of the dimeric RXRα contains a total of 229 exchangeable amide hydrogens. Global mass changes in the nonliganded protein and in the protein−ligand complex following H/D exchange were determined by analyzing the intact protein by LC-ESI MS. The incorporation of deuterium at amide sites (side chain and C- and N-terminal deuteriums are removed by back-exchange during LC separation) increased with incubation time in both the nonliganded protein and the protein−ligand complex. Deuterium was exchanged into approximately 140 (61%) of the amide hydrogens after 180 min (uncorrected for back-exchange). A mass difference of 18−24 Da or about 10% deuterium incorporation was observed between the nonliganded protein and the protein−ligand complex throughout the entire exchange period, 0.25−180 min (Figure 2). The fact that the mass difference remained constant provided strong evidence that the protein−ligand complex was stable in solution.

Peptic peptides were mass analyzed at various time points to probe the level of deuterium incorporated along the protein backbone in both the protein and the protein−ligand complex. These results were used to locate where deuterium incorporation between the two protein forms was different. Digestion with immobilized pepsin produced approximately 65 peptic peptides (Figure 3), which covered 98% of the protein sequence.

The percentage deuterium exchange-in into nonliganded protein as a function of time (0.25, 1, 5, 30, 90, and 180 min) is clearly different for different regions of the protein (Figure 3). The N-terminal region (fragment 219−233) was found to exchange very rapidly with over 85% amide

FIGURE 3: Amino acid sequence and peptic peptides of the human RXRα LBD. The first three residues (GSH) were introduced in the cloning procedure. The location of α-helices and *β*-strands are based on analysis of the X-ray coordinate file using the DSSP program. The location of residues that interact with the bound 9-*cis*-RA as defined by the X-ray structure are identified by solid red circles. The color coded deuterium incorporation for the unliganded RXRα homodimer along the protein backbone (percent) is shown for the six different time points.

hydrogens exchanging within the first 15 s. The fast exchange in this region is not surprising as the partial sequence is unstructured. The fragment 439−449 that is part of the long α-helix 12 containing nine amide hydrogens exhibited very fast exchange, indicating that the helix is highly accessible to solvent and hydrogen bonding is weak. Loop H11−H12 and the C-terminus also showed fast exchange, indicating that the entire C-terminal region of nearly 30 amino acid residues is exposed or is rapidly equilibrating with an exposed conformation.

Three other relatively fast-exchanging regions involving α-helices, *β*-strands, and loops were studied. One of these is located in the region between aa 241−254 that includes helix 2 and H1−H2 loop (Figure 3). This segment is highly exposed to solvent, and the hydrogens are, therefore, expected to exchange rapidly. Fragments that include aa 258−279 contain a large section of helix 3 that has four aa residues that are involved in binding 9-*cis*-RA. The region involving partial sequence aa 320−346 comprises *β*-turns 1 and 2, helix 6, and the N-terminal part of helix 7 that also contains residues that bind 9-*cis*-RA.

Each subunit of the native RXRα homodimer is a three-layered antiparallel α-helical sandwich as shown in the crystal structure (Figure 4) (*24*). The slow-exchange regions were found to be mainly in the core of this sandwich that encompasses helices 4, 8, and 9 (Figures 3 and 4A). The residues located in the center of these helices showed deuterium incorporation of less than 15% after 180 min exchange-in (Figure 3). Helix 5 is also located in the core of the sandwich, but in comparison to helices 4, 8, and 9, it exhibited somewhat faster hydrogen exchange. The slow exchanging region is not limited to the sandwich core; however, relatively slow exchange was also observed for helix 10, which is located in the outer layer of the sandwich structure (Figure 4).

Different rates of deuterium incorporation were also observed in different parts of secondary structural segments. These differences are often associated with the presence of one or more residues that are involved in binding 9-*cis*-RA. For example, the region around the N-terminus of helix 7 (aa 341−346), which contains amino acids V_{342} and I_{345} that interact with bound 9-*cis*-RA, exchanges hydrogens rapidly, but the middle region of helix 7 and the region around the C-terminus exchange relatively slowly. In helix 11, the region around the C-terminal part (aa 431−438) that binds the ligand at C_{432} and H_{435} exhibits fast hydrogen exchange, but the N-terminus undergoes slow exchange. The C-terminal part of helix 5 and the second 3_{10} helix (aa 313−319) also exhibit relatively fast exchange as compared to the N-terminal part of helix 5 or the first 3_{10} helix region (Figure 3). This region also contains a binding residue (R_{316}). Finally, helices 2, 3, 6 ,and 12, which, according to crystallographic analysis,

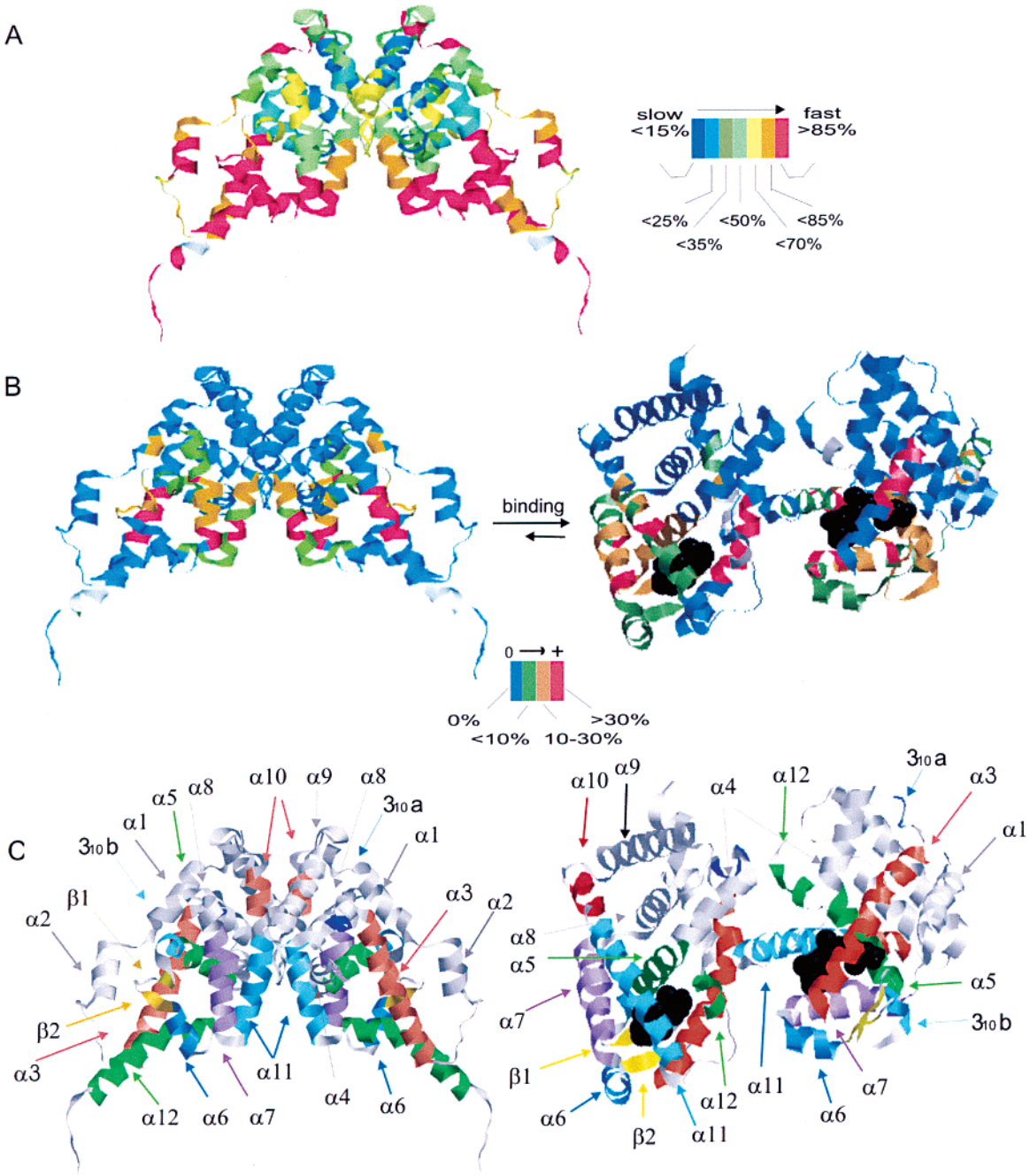

FIGURE 4: Ribbon plots of unliganded human RXRα LBD and the complex with 9-*cis*-retinoic acid based on the crystallographic data (*2*, *5*). The relative exchange rates for the free protein are shown in panel A, and the regions in which deuterium content changed at an assay time of 5 min are shown in panel B for the free protein (left) and the protein-9-*cis*-RA complex (right). The location of secondary structural elements for the free protein (left) and the complex with 9-*cis*-retinoic acid (right) are shown in panel C. In panels B and C, the bound 9-*cis*-RA is shown in black.

undergo major rearrangements after binding of 9-*cis*-RA (*25*), exhibit very fast hydrogen exchange. These segments are located near the surface and so are especially accessible to solvent.

The results for hydrogen exchange in the presence and absence of 9-*cis*-RA are shown in Figure 5 for a representative group of peptides obtained from a peptic digest of the RXRα homodimer. Deuterium levels in these peptic fragments were analyzed by directly coupled HPLC ESI-MS. Fragment 373−388 exhibited identical H/D content in the free protein and the protein−ligand complex over the measured time period, indicating that the presence of ligand did not alter solvent accessibility in this region. Fragments 271−278 and 313−319, shown to contain binding site residues by crystallographic analysis, exhibit significant decrease in the amount of deuterium incorporated when bound to 9-*cis*-RA. These results agree with the model provided by crystallographic data. Fragment 423−429 also showed protection in the RXRα−9-*cis*-RA complex. The amino acids in this fragment are not in direct contact with ligand but are located near C_{432} and H_{435} residues that do contact with bound ligand. Thus, it seems likely that some type of structural changes resulting in protection against H/D exchange took place in this region after ligand bound.

Significant differences in H/D content were observed in corresponding peptides from nonliganded protein and the

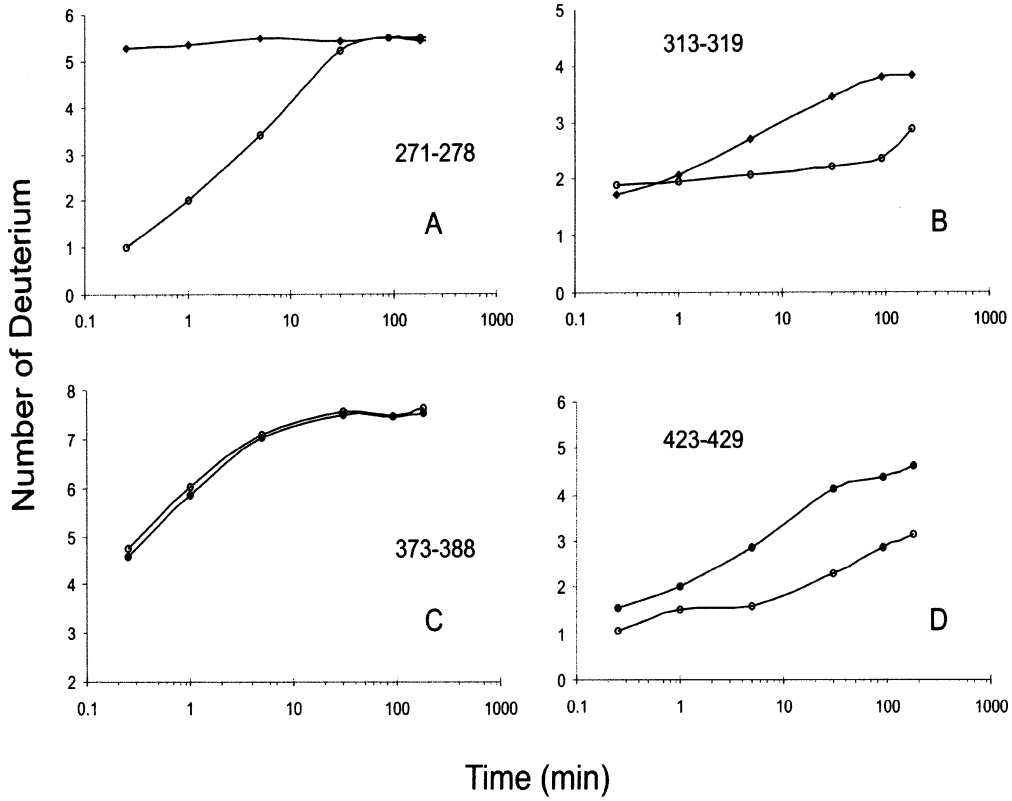

FIGURE 5: Deuterium levels at backbone amides as a function of time in four representative peptic fragments of the human RXRα homodimer LBD: (A) 271−278, (B) 313−319, (C) 373−388, and (D) 423−429. Solid circles represent the deuterium content of the free protein, and open circles show the deuterium content of the protein-9-*cis*-RA complex. Data points are an average of two experiments with a typical difference of 5−10% between experiments. No correction was made for proton back-exchange.

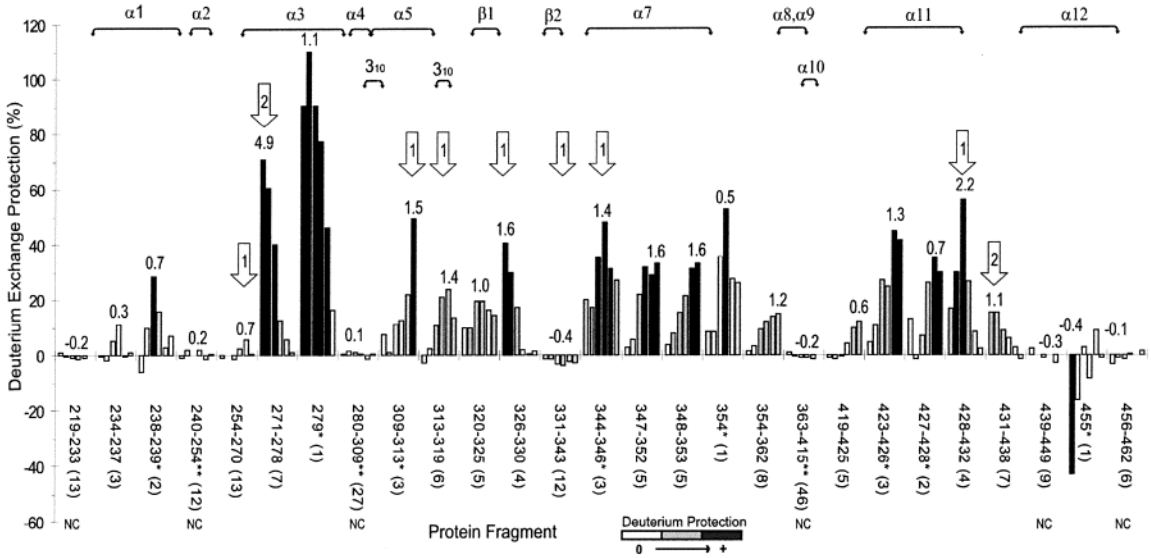

FIGURE 6: Protection against deuterium exchange in RXRα peptic peptides. The difference in deuterium content between free RXRα and the 9-*cis*-RA complex at six time points (0.25, 1, 5, 30, 90, and 180 min, left to right) for each peptic fragment is shown as a series of vertical bars. Data are the average of two experiments with a range of about 5−10% between experiments. The total number of exchangeable amide hydrogens is shown in parentheses below the fragment number, and the maximum observed difference in deuterium incorporated is shown above each time course. The significance of the observed deuterium difference is indicated by shading of the bars: clear indicates an insignificant difference of less than 0.3 Da, and highly significant differences are indicated by black bars. Where applicable, the number of residues in the fragment that interact with the bound ligand are shown within an open arrow. The elements of secondary structure are shown at the top of the figure. NC indicates no change, * indicates that the information was deduced from overlapping peptides, and ** indicates that the information was obtained by merging sequential peptides.

protein−ligand complex after exposure to identical hydrogen exchange conditions (Figure 6). The highest absolute deuterium difference at the experimental time period is given above each fragment. From these results, it can be seen that reduced deuterium levels occur in major stretches of the sequence in the protein−ligand complex relative to the free protein. The results indicate that the ligand sterically obstructs solvent access around the binding sites and hinders the exchange. Protection against exchange of amide hydrogens is, however, also evident in other parts of the complex as

reflected by the reduced levels of deuterium in peptides in these regions.

There are about 18 peptides exhibiting deuterium level decreases ranging between 5 and 70% that change with time after the binding of 9-*cis*-RA (Figure 6). In addition, about 53% of the residues in the protein−ligand complex show almost no difference in H/D content within the experimental exchange-in time period, which suggests that these segments experienced no conformational changes or that any changes that occurred cannot be measured by H/D exchange. These segments include the N-terminus (aa 219−233); the segment that includes helix 2 (aa 240−254); the C-terminus of helix 3; the first 3_{10} helix, helix 4; the N-terminus of helix 5 (aa 280−309); an extensive segment that covers helices 8, 9, the N-terminus of helix 10, and the connecting loops (aa 363−415); the segment that includes part of helix 12 (aa 439−449); and the C-terminus (aa 456−462).

Overlapping peptic peptides were sometimes found useful for increasing the spatial resolution of sites undergoing hydrogen exchange, although it was found essential that back-exchange be small and similar. The back-exchange for some small fragments consisting of two to three amino acids, for example, can be extensive, thereby precluding their usefulness for mapping structural changes. On the other hand, for fragment 234−239, in which back-exchange was ∼17%, the deuterium content in the complex was found reduced in centroided mass by 0.7 Da at 5 min exchange-in time, whereas no change occurred in fragment 234−237 with ∼16% back-exchange. These results led to the conclusion that the reduced deuterium content in the liganded protein was localized at residues aa 238−239. This contrasts with results for fragment 237−240 from the liganded and non-liganded proteins, where no difference in deuterium content was observed, but back-exchange was 50%.

Deuterium exchange-in on residues L_{279}, V_{354}, and L_{455} was obtained from fragments 271−278 and 271−279, 353−362, and 354−362, 454−462, and 455−462, respectively. The deuterium content in amino acids, L_{279} and V_{354}, located near the ligand binding site showed a large decrease in deuterium content after binding 9-*cis*-RA. X-ray data showed that L_{279} moves slightly (1.37 Å) from its original position, and V_{354} moves significantly when ligand binds (*21*). Parameters calculated from the X-ray coordinates for these residues indicate that they lie deeper and that solvent accessibility surface area is reduced in the complex (Table 1). According to X-ray analysis, L_{455}, which is located at the end of helix 12 in the free protein, is repositioned in the protein−ligand complex. In solution, it exhibited greater solvent exposure after ligand binding.

Table 1: Comparison of the Deuterium Level Difference in Peptic Fragments from the Free Protein and the Protein−Ligand Complex at 5 Min and Changes in the Structural Parameters Hydrogen Bonding, Solvent Accessible Surface Area, and Depth for Free and Ligand Occupied RXRα[a]

	fragment	D-level change (%)	ΔSAS (%)	ΔH-bond (#)	Δdepth (%)
α1	225−233	0.0	**−3.2**	−1	0.0
	234−237	−5.2	−1.6	−1	**+1.7**
	238−239	−28.6	+1.4	**+1**	0.0
α3	271−278	−40.1	**−17.2**	−6	**+15.0**
	279	−90.4	−3.4	0	**+28.6**
	280−289	0.0	**+2.0**	+1	+8.9
α4	290−296	0.0	**−6.4**	+1	**+6.4**
	297−300	0.0	−9.6	**0**	+14.0
	301−309	0.0	−8.0	**0**	**+3.3**
α5	309−312	−11.2	−3.4	0	−10.3
	313−319	−10.6	+0.5	**+1**	−4.8
β1	320−325	−19.4	+3.8	**+1**	−9.0
α6	326−330	−17.3	+36.4	**+1**	−21.4
β2	331−343	+3.2	**−0.3**	−2	**−3.3**
	344−346	−35.3	+9.3	**+1**	−16.1
α7	347−352	−22.0	−0.2	0	0.0
	348−353	−5.4	+0.5	0	+1.9
	354	−35.5	**−25.9**	**+1**	**+66.7**
	354−362	−9.2	+3.7	**+1**	0.0
α8	363−367	0.0	+7.4	−1	**−4.2**
	368−372	0.0	**−0.5**	**0**	**0.0**
	373−390	0.0	**+0.3**	−1	**0.0**
α9	391−397	0.0	**+2.9**	**0**	**−5.3**
	395−400	0.0	**−0.5**	**0**	**−3.1**
α10	401−415	0.0	**−0.9**	+1	**0.0**
	419−425	0.0	**−4.9**	**0**	**+6.0**
α11	423−426	−27.0	−1.4	0	+3.6
	427−428	−6.9	−4.0	0	+7.8
	428−432	−55.8	+6.1	0	−13.4
	431−438	−8.6	**−11.4**	**+1**	+1.9
12	439−449	0.0	+26.7	**0**	−17.4
	455	0.0	−45.9	**0**	+34.2

[a] The bold numbers in the column for a structural parameter indicate a positive correlation.

DISCUSSION

Specific residues are involved in the interaction between 9-*cis*-RA and RXRα LBD homodimer as shown by crystallographic data. The ligand binding region is buried within the protein in a hydrophobic environment located between the β-sheet and helices 3, 5, 11, and 12 (Figure 4). The residues involved in binding are located in peptides containing the N-terminal half of helix 3 (aa 264−275); the loop between the two β-sheets; the N-terminus of helix 7, helix 5, and the second 3_{10} helix part (aa 313−316); and the C-terminus of helix 11 and loop between helices 11−12 (aa 432−435, Figure 3, red dots). The regions encompassing these residues generally undergo fast H/D exchange when no ligand is present, indicating that the backbone amide bonds are substantially accessible to solvent and/or hydrogen bonding is relatively weak. Most of the hydrogen exchange in these regions is complete within 5 min; the β-sheet within 15 s. Regions of the protein that are not involved in forming the ligand binding site often exchange slowly (Figure 3) and appear to be located in those parts of the binding cavity that appear to provide structural rigidity. Residues in contact with the ligand and immediately adjacent residues exchange hydrogens rapidly suggestive of the structural flexibility needed to undergo a conformational change when binding ligand.

Examination of the difference in the time-dependent deuterium uptake between protein and liganded protein (Figure 6) reveals that there are six regions containing a total of 103 amide hydrogens per subunit that show no change in deuterium incorporation and none of these includeamino acids that interact with the bound ligand. There are nine peptides containing amino acids that interact with 9-*cis*-RA. Many showed an initial difference of as much as 70% deuterium content relative to the peptides from the non-liganded protein such as fragment 271−278. Others seemed to show a maximum reduction in deuterium level after 5, 30, or 90 min exchange-in time, and one region, aa 310−

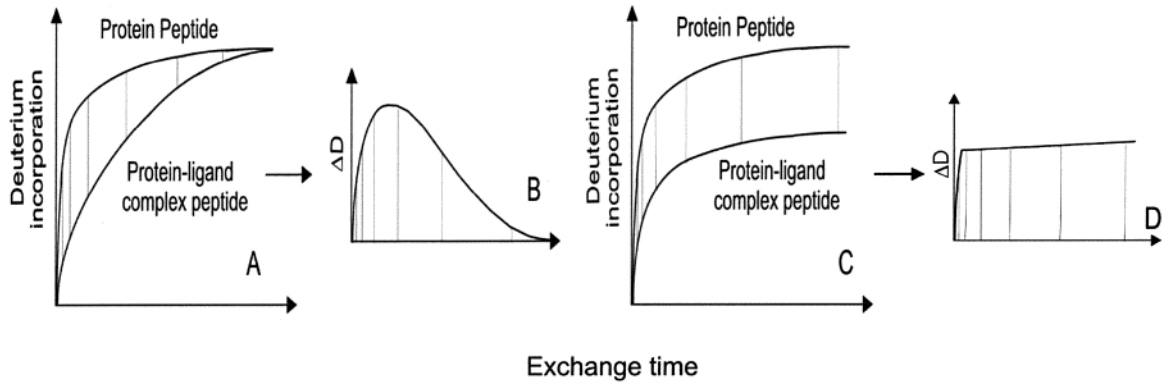

FIGURE 7: Representation of the time dependence of the difference in deuterium uptake between free protein and protein−ligand complex. Panel A shows the time dependence of deuterium uptake for a system in which the ligand protects against H/D exchange, but both free protein and the protein−ligand complex reach equilibrium within the experimental time frame. This type of behavior gives rise to the difference curve in deuterium uptake versus time shown in panel B. In panel C, the free protein equilibrates rapidly, but the protein−ligand complex does not reach equilibrium within the experimental time frame. The difference in deuterium uptake versus time for this system is shown in panel D.

313, initially underwent hydrogen exchange at about the same rate as its counterpart in the nonliganded protein, then diminished with time. Eight peptides containing no interacting residues also showed relative differences in deuterium content, most displaying the same deuterium incorporation pattern as segment aa 310−313.

These results can be explained on the basis of differential rates of exchange between the nonliganded protein and the liganded protein. For the nonliganded protein, there is initially a rapid uptake of deuterium that gradually levels off as the maximum numbers of exchangeable amide hydrogens is approached. In the ligand−protein complex, the rate of exchange is reduced, but given enough time, the numbers of hydrogens that exchange will eventually be the same as in the nonliganded protein. Thus, a differential pattern of deuterium uptake appears (Figure 7A), which shows up first as an increasing difference, reaching a maximum before decreasing to zero again (Figure 7B). This behavior is reflected by fragments 313−319, 320−325, and 429−432, while others, fragments 271−278 and 432−438, display only the downslope part, which means that that region of free protein from which the peptide was derived exchanged so much faster than its counterpart in the ligand−protein complex at the earliest time point (i.e., 15 s), resulting in a maximum difference in deuterium incorporation before the difference diminishes at the later time points. Almost all peptides containing amino acids that formed the ligand binding site displayed one of these two patterns.

Finally, there are peptides representing regions of the protein and protein−ligand complex in which the deuterium incorporation is initially the same, but with time a widening gap appears as the relative deuterium uptake diminishes in the complex (Figure 7C). The apparent deuterium content should merge given enough time, but this may not be evident within the time frame of the experiment (Figure 7D), in which case a maximum difference in the numbers of hydrogens undergoing equilibrium exchange is displayed. Regions of the liganded protein that are not involved in binding of 9-*cis*-RA tend to show this pattern. These slower exchanging segments consist of fragments 347−352 and 353−362 that contain helix 7 and the H7−H8 loop and fragments 419−425 and 423−429 that encompass helices 10 and 11 and the intervening loop.

It is known from crystallographic data that when agonists bind to the RXRα LBD, the β-sheet and helices 5, 6, and 10 are shifted slightly, and helices 11 and 12, the H11−H12 loop, and the segment between helices 1 to 3 undergo major rearrangements (Figure 4). X-ray data also indicate that helix 2 acts as a molecular spring, providing assistance in the movement of helix 3 toward the ligand. The large movement of these domains serves to position helix 12 so that it closes the ligand binding pocket. The region aa 439−462 that includes almost all of helix 12 shows no change in deuterium incorporation except for an apparent accelerated rate at L_{455} in the first 5 min. Thus, there appears to be no major change in solvent accessibility, hydrogen bond strength, or other physical parameters that govern hydrogen exchange, despite the major participation of this segment in closing the ligand binding pocket. The region aa 280−309 that encompasses part of helix 3, the first 3_{10} helix, helix 4, and part of helix 5 also shows no difference in deuterium uptake.

In helix 11 (aa 422−434), the conformational changes are more complex. Crystallographic data indicate that major structural rearrangement occurs in this segment upon binding 9-*cis*-RA (*25*), but secondary structural analysis and three-dimensional structure superposition analysis, based on X-ray data, indicated that the major rearrangement occurred in the C-terminal part of helix 11 as the H11−H12 loop becomes part of the helix (Figure 4). The residues from K_{431} to L_{436} are shifted slightly (1−2 Å) away from their original positions upon ligand binding, whereas the remainder of helix 11 (aa 422−430) is not significantly affected according to X-ray data and three-dimensional structure superposition analysis. However, a large difference in H/D content was observed between the free protein and the liganded protein within fragments covering aa 423−432. A significant H/D content difference was also observed in fragments 238−239, 320−325, and 419−425, suggesting that conformational changes occurred in these regions when 9-*cis*-RA binds to the protein in solution. These results were not predicted by the crystallographic data.

The decreased deuterium incorporation particularly in helices 10 and 11 may be a result of reduced solvent accessible surface area, a reduction in protein breathing, increased hydrogen bonding, increased depth, or a combination of these parameters. An attempt to correlate changes in

deuterium incorporation with changes in calculated structural parameters was reasonably successful (Table 1). For example, changes in parameters such as depth and solvent accessibility correlated well with the hydrogen exchange results for fragments covering aa 419−428. In helix 7, the calculated parameters indicate that there is a significant reduction in solvent accessibility surface for L_{354}; two new hydrogen bonds are also predicted in fragment 354−362. The significant decrease in relative deuterium content observed in fragment 271−278 of the complex correlates with a large decrease in calculated solvent accessible surface area and an increase in residue depth. In fragments covering the region aa 363−415, which encompasses helix 9, there was no net change in deuterium incorporation in the protein−ligand complex, and calculations based on X-ray coordinates suggest there would be little or no change in solvent accessibility surface, depth, or hydrogen bonding (Table 1). These correlations are consistent with the overall conformational changes in the liganded protein on the basis of crystallographic data.

But exceptions also exist. For example, a considerable deuterium content decrease was observed for aa 423−426 in helix 11 when 9-*cis*-RA binds, suggesting a conformational change. Conformational changes in this region were also confirmed by tryptic cleavage analysis (*26*). However, none of the above parameters can explain the protection against deuterium exchange found in this fragment when ligand binds. X-ray crystallographic coordinates of atoms in the structures of proteins can be used as close approximations for the locations of these atoms in solution, but proteins are probably more flexible in solution. The present study is consistent with this expectation, although there is no information about the relative contribution of these parameters and protection strength for each factor.

It is seen that H/D exchange can provide supplemental information not available from X-ray data. Global hydrogen/deuterium exchange on the intact RXRα LBD homodimer with and without 9-*cis*-RA showed that 18−24 residues were affected by binding in the complex. The considerable decrease in deuterium content that was observed in aa 238−239, 423−426, and 427−428 from the complex (Figure 6) was not evident in the crystal structure, and superposition of the three-dimensional structure suggested that these residues did not change position significantly (distance moved less than 0.8 Å, RMSD less than 0.3 Å). Intact segment movement of helices 2 and 12, which is precisely described in the crystal structure, underwent little deuterium exchange difference in the corresponding fragments of the free protein and the protein−ligand complex, except for L_{455}, which became more solvent exposed. Major conformational changes on a segment may not be associated with a change in solvent accessibility, protein dynamics, or hydrogen bond strength, in which case detecting these changes by amide H/D exchange cannot be achieved.

In conclusion, deuterium incorporation into intact protein exhibited a considerable decrease due to binding of 9-*cis*-RA, suggesting that a conformational change occurred in which about 20 backbone amide hydrogens become protected against exchange by deuterated solvent. These results are consistent with hydrodynamic studies by Egea (*2*), who showed that the RXRα homodimer becomes more compact upon binding ligand. Regions of the protein in contact with the ligand as suggested by X-ray data were detected by the H/D exchange technique, and regions remote from the binding sites showing a change in environment after ligand binding were also detected. The present results demonstrate the unique power of H/D exchange and analysis by mass spectrometry in characterizing structural features of proteins in solution that crystallographic data cannot provide.

ACKNOWLEDGMENT

We acknowledge the support of the nucleic acid and protein core and the mass spectrometry core in the OSU Environmental Health Sciences Center (NIH/NIEHS 00210). We are grateful to Dr. Akshay Bhinge for depth calculations and to Dr. William Bourguet for the RXR LBD homodimer nonliganded coordinate file. We thank Pascal Egea and Dino Moras (Laboratoire de Biologie et de Génomique Structurales, Institut de Génétique et de Biologie Moléculaire et Cellulaire, Illkirch, France) for the kind gifts of bacterial expression vectors encoding the ligand binding domains of RAR and RXR.

REFERENCES

1. Chambon, P. (1994) *Semin. Cell Biol. 5*, 115−25.
2. Egea, P. F., Rochel, N., Birck, C., Vachette, P., Timmins, P. A., and Moras, D. (2001) *J. Mol. Biol. 307*, 557−576.
3. Gampe, R. T., Jr., Montana, V. G., Lambert, M. H., Wisely, G. B., Milburn, M. V., and Xu, H. E. (2000) *Genes Dec. 14*, 2229−2241.
4. Bourguet, W., Ruff, M., Chambon, P., Gronemeyer, H., and Moras, D. (1995) *Nature 375*, 377−382.
5. Egea, P. F., Mitschler, A., Rochel, N., Ruff, M., Chambon, P., and Moras, D. (2000) *EMBO J. 19*, 2592−2601.
6. Torchia, J., Glass, C., and Rosenfeld, M. G. (1998) *Curr. Opin. Cell Biol. 10*, 373−383.
7. Freedman, L. P. (1999) *Cell 97*, 5−8.
8. Gampe, R. T., Jr., Montana, V. G., Lambert, M. H., Miller, A. B., Bledsoe, R. K., Milburn, M. V., Kliewer, S. A., Willson, T. M., and Xu, H. E. (2000) *Mol. Cell 5*, 545−555.
9. Englander, S. W., Mayne, L., Bai, Y., and Sosnick, T. R. (1997) *Protein Sci. 6*, 1101−1109.
10. Raschke, T. M., and Marqusee, S. (1998) *Curr. Opin. Biotechnol. 9*, 80−86.
11. Engen, J. R., Gmeiner, W. H., Smithgall, T. E., and Smith, D. L. (1999) *Biochemistry 38*, 8926−8935.
12. Anand, G. S., Hughes, C. A., Jones, J. M., Taylor, S. S., and Komives, E. A. (2002) *J. Mol. Biol. 323*, 377−386.
13. McCallum, S. A., Hitchens, T. K., Torborg, C., and Rule, G. S. (2000) *Biochemistry 39*, 7343−7356.
14. Engen, J. R., and Smith, D. L. (2001) *Anal. Chem. 73*, 256A−265A.
15. Kaltashov, I. A., and Eyles, S. J. (2002) *Mass Spectrom. Rev. 21*, 37−71.
16. Bradford, M. M. (1976) *Anal. Biochem. 72*, 248−254.
17. Kabsch, W., and Sander, C. (1983) *Biopolymers 22*, 2577−2637.
18. McDonald, I. K., and Thornton, J. M. (1994) *J. Mol. Biol. 238*, 777−793.
19. Fraczkiewicz, R., and Braun, W. (1998) *J. Comput. Chem. 19*, 319−333.
20. Chotia, C. (1975) *J. Mol. Biol. 105*, 1−14.
21. Zemla, A. (2003) *Nucleic Acids Res. 31*, 3370−3374.
22. Chakravarty, S., and Varadarajan, R. (1999) *Structure 7*, 723−732.
23. Losi, A., Wegener, A. A., Engelhard, M., Gartner, W., and Braslavsky, S. E. (1999) *Biophys. J. 77*, 3277−3286.
24. Steinmetz, A. C. U., Renaud, J.-P., and Moras, D. (2001) *Annu. Rev. Biophys. Biomol. Struct. 30*, 329−359.
25. Egea, P. F., Klaholz, B. P., and Moras, D. (2000) *FEBS Lett. 476*, 62−67.
26. Leid, M., unpublished data.

BI030183C